Addressing stability challenges of using bimetallic electrocatalysts: the case of gold-palladium nanoalloys

-

Supporting Information

Enrico Pizzutilo[a*], Simon J. Freakley[b], Simon Geiger[a], Claudio Baldizzone[b], Andrea Mingers[a], Graham J. Hutchings[b], Karl J. J. Mayrhofer[a,c,d], Serhiy Cherevko[a,c*]

[a]*Department of Interface Chemistry and Surface Engineering, Max-Planck-Institut für Eisenforschung GmbH,*
Max-Planck-Strasse 1, 40237 Düsseldorf, Germany

[b]*Cardiff Catalysis Institute, School of Chemistry, Cardiff University, Main Building, Park Place, Cardiff, CF10 3AT*

[c] *Forschungszentrum Jülich GmbH, Helmholtz Institute Erlangen-Nürnberg for Renewable Energy (IEK-11), Egerlandstr. 3, 91058 Erlangen, Germany*

[d]*Department of Chemical and Biological Engineering, Friedrich-Alexander-Universität Erlangen-Nürnberg, Egerlandstr. 3, 91058 Erlangen, Germany*

[*]*Corresponding authors: pizzutilo@mpie.de s.cherevko@fz-juelich.de*
Tel.: +49 211 6792 160, FAX: +49 211 6792 218

SUPPORTING INFORMATION

S1 TEM Characterization

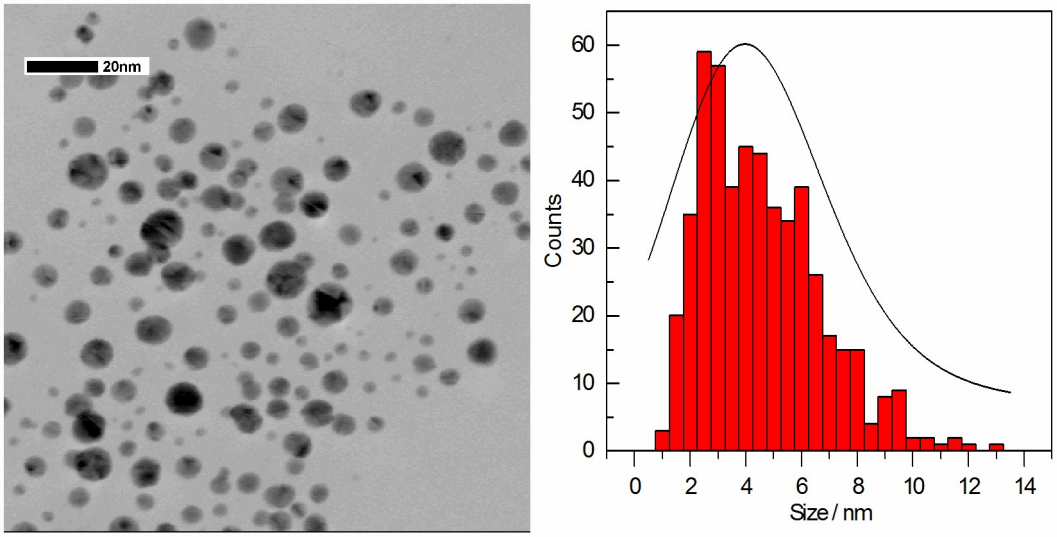

Figure S1.1 Representative bright field TEM micrographs (left) and statistic particle size distribution(right) showing Au sol gel nanoparticles deposited on a lacey carbon TEM grid.

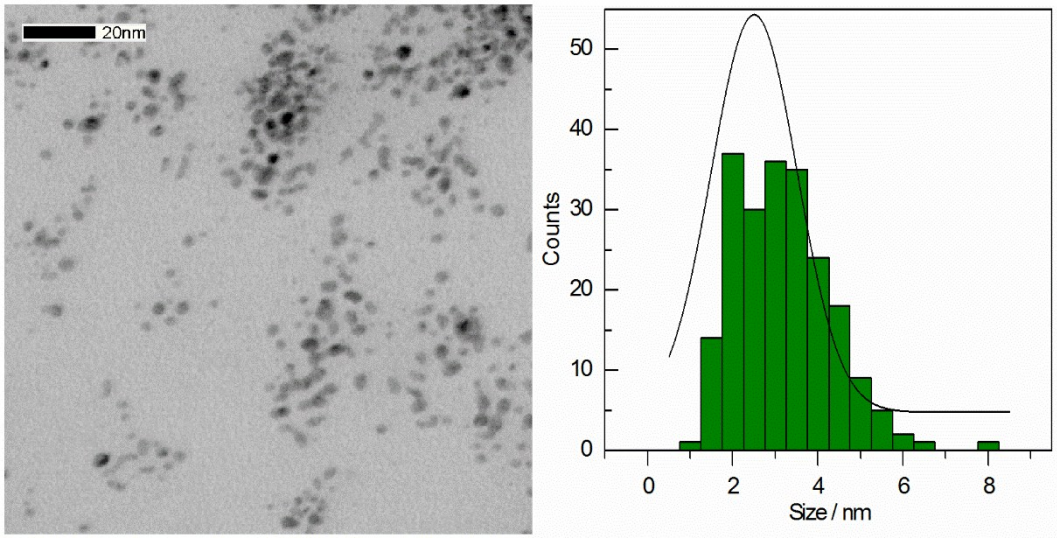

Figure S1.2 Representative bright field TEM micrographs (left) and statistic particle size distribution(right) showing Pd sol gel nanoparticles deposited on a lacey carbon TEM grid.

In a precedent study [1] XEDS spectra obtained from individual particles showed characteristic Au M lines and Pd L lines confirming that intimately mixed AuPd alloys had been formed rather than physical mixtures of pure Au and Pd particles. However, considerable systematic composition variations as a function of particle size were shown from the XEDS spectra obtained for individual particles.
.

S2 ECSA At

To measure the total surface area two different methods are considered: (I) one based on the mean particle size and the catalyst load, (II) one based on the double layer capacity (Figure S2).

The surface area of the Pd/C nanocatalyst is estimated (Table 1 in main text) from the TEM average sizes following the calculation described in [2]. In our case a spherical geometry was assumed, whose volume is:

$$V=4/3\ \pi\ r^3 \qquad S1.1$$

Where r is the radius (half of the mean particle size as in Table 1).
The surface area is:

$$A=4\ \pi\ r^2 \qquad S1.2$$

Thus, the specific surface area is:

$$ECSA=3/(r*\rho) \qquad S1.3$$

Where ρ is the crystallographic density of palladium (ρ_{Pd}=12.02 g cm^{-3}):
The total metal surface area was calculated as follow:

$$A_t=ECSA*m \qquad S1.4$$

Where m is the mass of metal (2 ng_{metal})

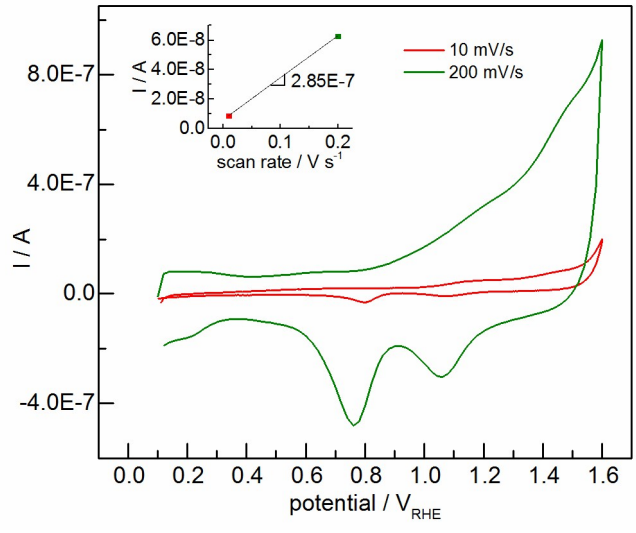

Figure S2 Recorded cyclic voltammetry for AuPd catalyst (1 layer) at 10 and 200 mV s^{-1}. From the slope of the current values is derived the capacity (inset).

The surface area was found to be around 0.002 cm^2 with the first method and around 0.005 cm^2 with the second (considering a value of 44.5 µF cm^{-2} [3]). The difference could be

considered within the error due to (I) the ambiguity in the evaluation of the capacity, (II) the difficulty in estimating precisely the exact loading and (III) the overestimation of the capacity that includes also the glassy carbon support.

For this study, the normalization was done with total surface areas (A_t) reported in the paper in Table 1.

In binary alloys is also possible to estimate the surface area of the single metals with (I) surface oxide reduction charges (II), hydrogen under potential deposition (H_{UPD}) and (III) $CO_{stripping}$. The first two methods were discussed in the main text. $CO_{stripping}$ is efficacious for the determination of Pd surface area, however (I) the value of the charge of a monolayer is ambiguous, (II) Au seems to have an effect of $CO_{stripping}$ and (III) CO is known in literature to induce surface migration [4], which might alter the surface area composition and its estimation during the measurement.

For this study, we are more interested in the dissolution trends, therefore a precise determination of surface area composition is out of scope and only trends in oxide reduction charges are considered and presented (Figure 3).

S3 Dissolution during the first cycle

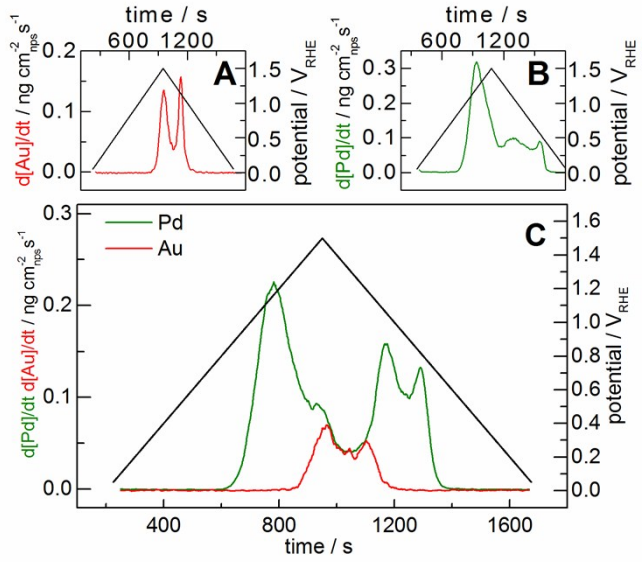

Figure S3.1 Dissolution profiles of (a) pure gold, (b) pure palladium and (c) gold-palladium alloy (all 4 layers) during a cyclic voltammogram between 0.05 and 1.5 V_{RHE} in Ar purged 0.1M $HClO_4$ with a scan rate of 2 mV s^{-1}. Flow rate is 193 µL min^{-1}.

In Figure S3.1 is shown the dissolution profile of pure gold, pure palladium and gold-palladium alloyed. Only the first cycle is here reported and for this measurement the dissolution was normalized with As (Table 1). The dissolved Pd and Au for the alloyed metal is approximately the half of the corresponding pure metal. Since this value is reported here normalized by the total surface area, we can derive that during the first cycle on the catalyst surface the amount of Pd and Au is close to the nominal 1:1 atomic ratio (in fact the normalized dissolution is approximately half of the pure metal).

In the next Figures S3.2-3 are shown and compared the onset potentials of Pd and Au (pure and alloyed nanoparticles).

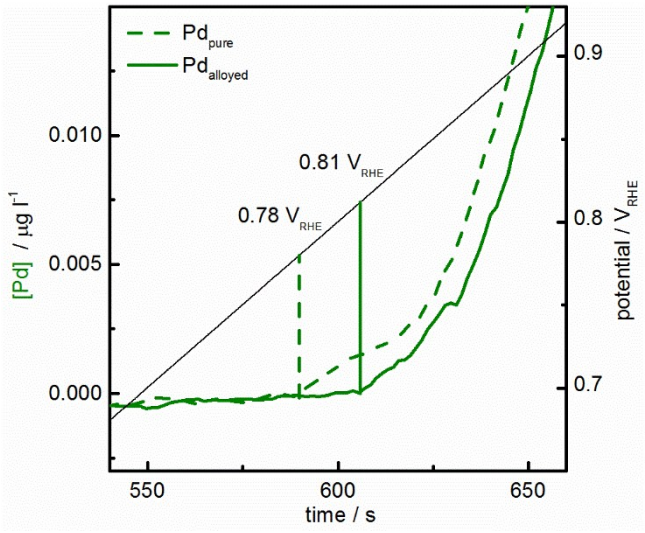

Figure S3.2 Comparison of dissolution onset potentials of Pd_{pure} and $Pd_{alloyed}$ nanoparticles.

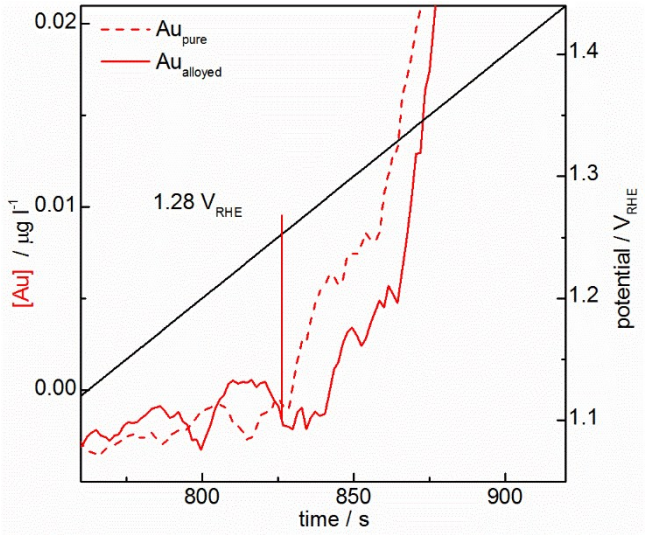

Figure S3.3 Comparison of dissolution onset potentials of Au_{pure} and $Au_{alloyed}$ nanoparticles.

S4 Upper Limit Potential

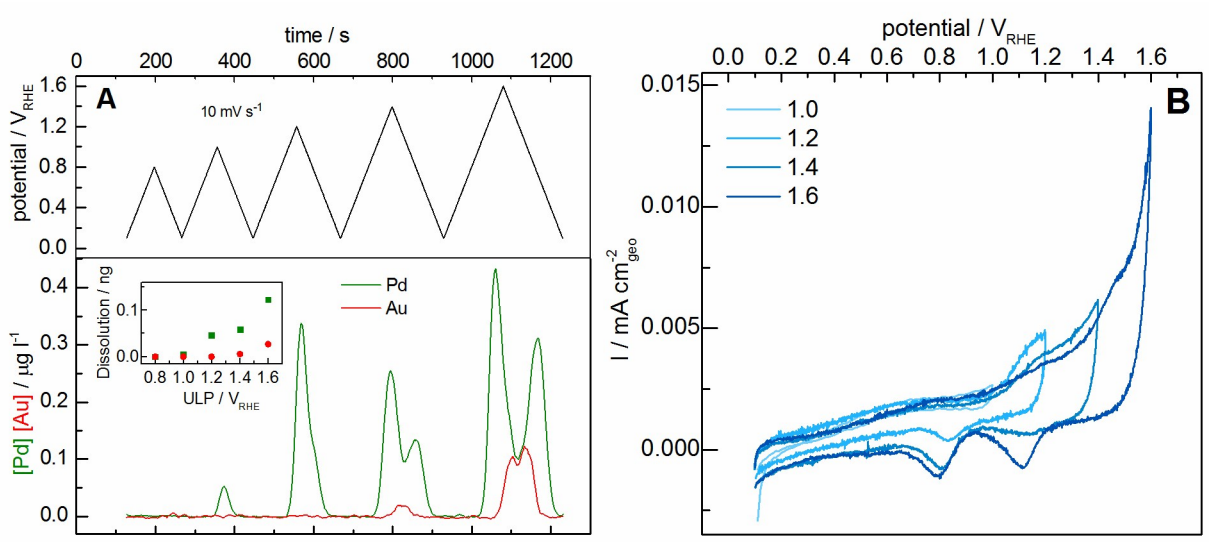

Figure S4 Several cycles to different upper limit potentials (ULP) with 10 mV s^{-1} for AuPd catalyst (1 layer) in 0.1M $HClO_4$. The corresponding Au and Pd dissolution profiles and the voltammograms are shown in (a) and (b), respectively.

A series of potential sweeps with increasing upper potential limit (UPL) (Figure S4) was applied to the prepared 1 layer AuPd electrode and the corresponding dissolution profiles and cyclic voltammograms are shown. Significant dissolution signal is observed when the potential is above 1.0 V_{RHE} and 1.4 V_{RHE} for Pd and Au respectively. Below a certain potential only a single peak is discernible, while at higher potentials are present two distinct peaks (corresponding to anodic and cathodic dissolution). This was already observed in the case of polycrystalline gold dissolution [5] and it is probably due to the enhancement of anodic dissolution. The amount of dissolved Au and Pd in every cycle, which corresponds to the area under the dissolution profiles, is shown in the inset of figure S4.1a and is increasing with the upper potential limits.

S5 Influence of medium in dealloying

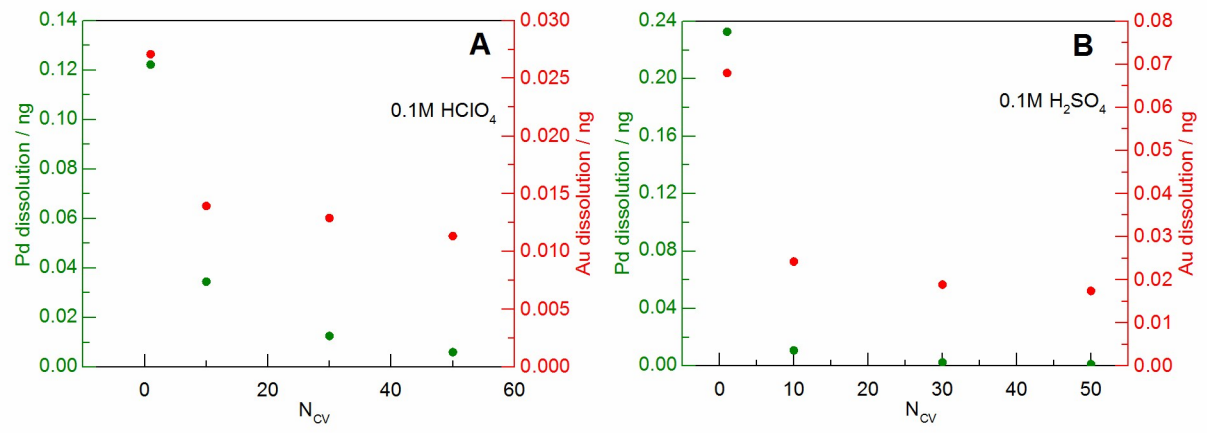

Figure S5.1 The total amount of metal dissolved per cycle corresponding to the slow cycles in perchloric acid (a) and sulfuric acid (b) of the measurement shown in Figure 3.

The dissolution profiles recorded during the slow cycles of the measurement described in Figure 3 are here shown for a comparison, with perchloric acid (Figure S5.1a) and sulfuric acid (Figure S5.1b).

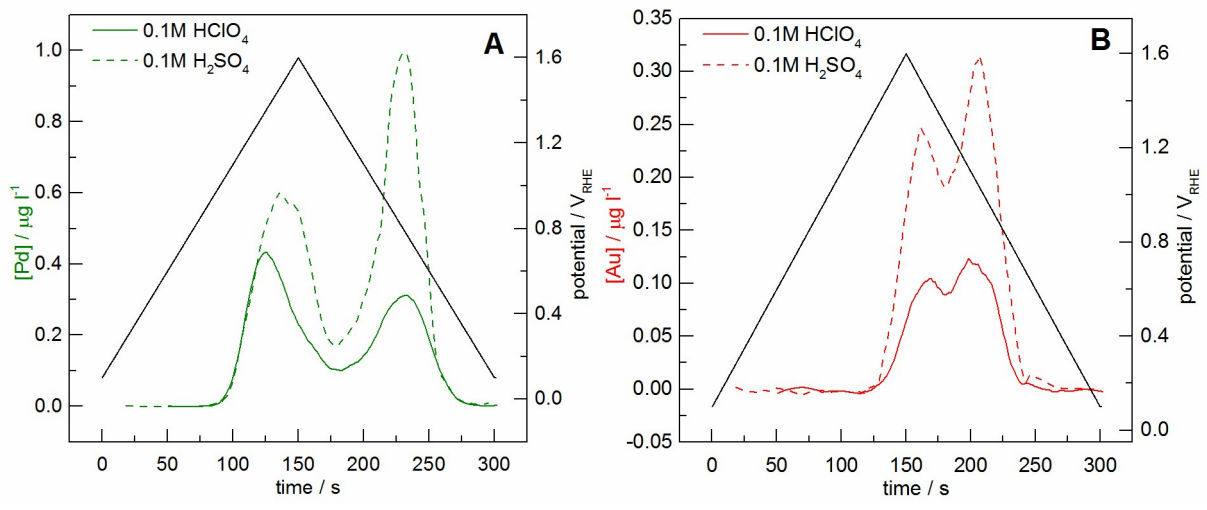

Figure S5.2 Comparison of (a) palladium and (b) gold dissolution profiles of AuPd nanoparticles (1 layer) in Ar purged electrolyte 0.1M $HClO_4$ (full line) and 0.1M H_2SO_4 (dotted line) during the first cyclic voltammogram between 0.1 and 1.6 V_{RHE} with a scan rate of 10 mV s^{-1} (see figure 3).

Comparing the Pd dissolution profiles during the first cycle in perchloric and sulfuric acid (Figure S5.2a) we can clearly conclude that the second is promoting the dissolution more than perchloric acid. The Pd dissolution onset potential is approximately the same in both acidic media. The behavior of Pd seems to be similar to the behavior of Pt. Indeed, no significant variation in the onset potential with pH or amount of sulfate or perchlorate anions was found previously also for polycrystalline platinum [6]. On the other side, our group showed that for polycrystalline gold there is a shift of almost 100 mV in the gold dissolution onset potential (≈1.3 V_{RHE} in sulphuric acid and ≈1.4 V_{RHE} in perchloric acid) [7]. The gold in the alloyed AuPd (Figure S5.2b) exhibits also a small shift in dissolution onset

potential of approximately 50 mV. However, the gold dissolution in both cases seems to start slightly before (≈ 1.25-1.30 V_{RHE}). For both metal higher dissolution in sulfuric acid are observed.

It seems that in perchloric acid for the first cycle anodic dissolution is more relevant, while in sulfuric acid is more important the cathodic dissolution. However, since the first cycle is the as prepared catalyst without any activation it is difficult to draw any conclusion and this need to be clarified. In both cases after a determined number of cycles Pd is completely dissolved and we have a gold enriched surface.

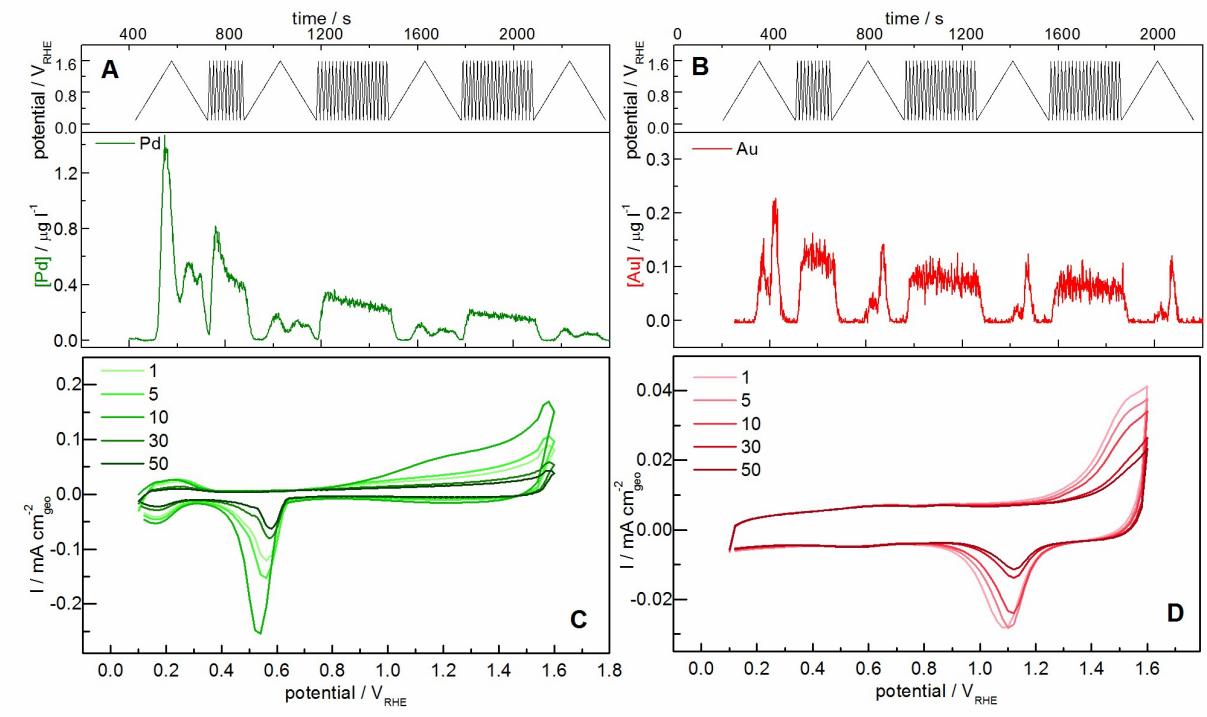

Figure S5.3 Dissolution profiles of (a) pure Au and (c) pure Pd nanoparticles (1 layer) in Ar purged 0.1M $HClO_4$ during 50 cyclic voltammograms between 0.1 and 1.6 V_{RHE} with a scan rate of 200 mV/s; some CVs at slower scan rate (10 mV/s) were as well recorded to compare the dissolution profiles with time (See SI). Corresponding SFC CVs (b,d)

As a reference in Figure S5.3 are shown the dissolution profile and voltammograms of pure Au and pure Pd in 0.1M $HClO_4$ (with the same protocol shown in Figure 3 for AuPd nanoparticles). In both cases during the degradation protocol the oxide reduction peaks are decreasing as well as the dissolution rates (in particular for Pd which is dissolving more). This is because the total surface area is decreasing due to the dissolution.

References

1. J. Pritchard, L. Kesavan, M. Piccinini, Q. He, R. Tiruvalam, N. Dimitratos, J. A. Lopez-Sanchez, A. F. Carley, J. K. Edwards, C. J. Kiely and G. J. Hutchings, *Langmuir*, 2010, **26**, 16568-16577.
2. J. S. Jirkovsky, M. Halasa and D. J. Schiffrin, *Phys Chem Chem Phys*, 2010, **12**, 8042-8052.
3. M. Lukaszewski and A. Czerwinski, *Electrochim Acta*, 2003, **48**, 2435-2445.
4. K. J. J. Mayrhofer, V. Juhart, K. Hartl, M. Hanzlik and M. Arenz, *Angew Chem Int Edit*, 2009, **48**, 3529-3531.
5. S. Cherevko, A. A. Topalov, I. Katsounaros and K. J. J. Mayrhofer, *Electrochem Commun*, 2013, **28**, 44-46.
6. A. A. Topalov, S. Cherevko, A. R. Zeradjanin, J. C. Meier, I. Katsounaros and K. J. J. Mayrhofer, *Chem Sci*, 2014, **5**, 631-638.
7. S. Cherevko, A. R. Zeradjanin, G. P. Keeley and K. J. J. Mayrhofer, *J Electrochem Soc*, 2014, **161**, H822-H830.